# Continuum Modeling of 1-D and 2-D Steady Detonation Wave Propagation in Porous High Explosives

Joshua R. Garno, Mark Short, Stephen J. Voelkel, Carlos Chiquete
Shock and Detonation Physics Group, Los Alamos National Laboratory
Los Alamos, NM, USA

## 1 Introduction

Polymer-bonded high explosives (HEs) are manufactured from molding powder composed of polymer-coated energetic crystals of reactive material that are pressed together to form a cohesive HE compact. Structural irregularity in HE molding powders results in granular resistance to compaction during pressing. Consequently, pressed HE contains residual porosity which typically occupies about 1-3% of the HE volume. Thermal and mechanical damage can also lead to the generation of significant additional porosity. Experiments indicate that HE detonation performance properties are sensitive to the initial HE density, or equivalently, initial porosity [1, 2]. The purpose of this work is to model the mechanisms by which porosity affects steady detonation propagation.

The basic modeling description of one-dimensional detonation involves a leading shock wave followed by a finite-length reaction zone, known as a Zeldovich-von Neumann-Döring (ZND) wave. The minimum steady wave speed is the Chapman-Jouguet (CJ) speed, wherein the flow at the end of the reaction zone is sonic in a frame traveling with the shock [3]. For multi-dimensional detonation, the wave speed is controlled by the energy release in the flow between the detonation shock and sonic surfaces, known as the detonation driving zone (DDZ) [4, 5, 6]. In porous HE, reaction and compaction processes occur simultaneously behind the detonation shock. The CJ speed then depends on the effect of reaction and compaction processes influencing the energy release in the 1-D wave. Compaction effects further complicate the DDZ structure in multi-dimensional flows.

In this work, a continuum-scale, compressible mixture modeling approach is used to examine the effects of initial HE porosity on steady detonation wave propagation. Residual porosity is not typically accounted for in HE models explicitly, rather its effects are implicit within the HE equation of state (EOS) and reaction rate models [5, 7]. Here, the HE is decomposed into reactive material and porosity components, enabling us to investigate the effects of initial porosity and finite-rate compaction processes on the reactive flow. A reactive burn model is used to resolve the details of the detonation reaction, while finite-rate compaction of HE material is captured by an evolution equation for the solid volume fraction. With given HE EOS and reaction rate models, the initial porosity and compaction viscosity are varied to explore their effects on steady 1-D and 2-D unconfined detonation wave propagation.

Correspondence to: jgarno@lanl.gov 

## 2 Model

The detonation flow in a porous HE is modeled by the Euler equations supplemented by evolution equations for reaction progress $\lambda_s \in [0,1]$ and volume fraction $\alpha_s \in (0,1]$,

$$\frac{\partial}{\partial t}\begin{Bmatrix}\rho\\ \rho\boldsymbol{u}\\ \rho E\\ \rho\lambda_s\\ \rho\alpha_s\end{Bmatrix} + \nabla\cdot\begin{Bmatrix}\rho\boldsymbol{u}\\ \rho\boldsymbol{u}\boldsymbol{u}^T + p\boldsymbol{I}\\ \rho\boldsymbol{u}(e+|\boldsymbol{u}|^2/2+p/\rho)\\ \rho\boldsymbol{u}\lambda_s\\ \rho\boldsymbol{u}\alpha_s\end{Bmatrix} = \begin{Bmatrix}0\\0\\0\\ \rho\Lambda\\ \rho\mathcal{F}\end{Bmatrix}, \tag{2.1a-e}$$

$$\rho = \alpha_s\rho_s, \quad p = \alpha_s p_s, \quad \boldsymbol{u} = \boldsymbol{u}_s, \quad e = e_s(v_s, p_s, \lambda_s) = \frac{p_s + A}{\gamma - 1}v_s - \lambda_s q_s, \tag{2.2a-d}$$

$$\Lambda = k p_s(1-\lambda_s)^{1/2}, \quad \mathcal{F} = \frac{\alpha_s(1-\alpha_s)}{\mu}p_s, \tag{2.3a,b}$$

where $\{\rho, \boldsymbol{u}, p, e\}$ are the density, velocity, pressure and specific internal energy of the porous HE mixture, subscript $\{\}_s$ denotes the state in the HE material (or solid), $\Lambda$ is the reaction rate, and $\mathcal{F}$ is the compaction rate. Additionally, $v = 1/\rho$ and $v_s = 1/\rho_s$ are the specific volumes of the mixture and solid, respectively, and $\alpha_v = 1 - \alpha_s$ is the porosity. The magnitudes of reaction rate constant $k$ and compaction viscosity $\mu$ determine the length scales of reaction and compaction processes, respectively [6, 8]. The present model formulation may be understood as the model for a gasless, porous solid as in [9], or similarly the 2PVL model in [10], with an additional equation for reaction progress in the solid. It is similar to a model used in [11].

The Tait EOS, (2.2d), and reaction rate model parameters are set according to the properties of non-porous HE, given by

$$\left.\begin{array}{c}\rho_{s0} = 2\text{ g cm}^{-3}, \quad A = 12.8\text{ GPa}, \quad \gamma = 3,\\ q_s = 3.24\text{ mm}^2\,\mu\text{s}^{-2}, \quad k \approx 0.05135906\text{ GPa}^{-1}\mu\text{s}^{-1}\end{array}\right\}, \tag{2.4}$$

which results in a CJ detonation speed $D_{CJ} = 8$ mm $\mu$s$^{-1}$.

One-dimensional, steady-state detonation wave structures are calculated using a variable-step ODE integration. Standard finite volume methods are used on a shock-fitted, shock-attached frame of reference to simulate unconfined detonation in two-dimensional planar HE slabs (Fig. 1). Spatial discretization is performed using a second order Lax-Friedrichs flux with a monotone-centered limiter, and temporal integration by a second order TVD Runge-Kutta method.

## 3 Results

Chapman-Jouguet solutions for steady propagating one-dimensional detonation waves in initially porous HEs are calculated by using the constant wave speed ($D_0$) conservation relations appropriate for equations (2.1a-c) along with the CJ (sonic flow) condition,

$$\rho U = -(\rho_0 D_0), \quad p = \rho_0 D_0^2\left(1 - \frac{\rho_0}{\rho}\right), \quad e - e_0 + \frac{1}{2}p\left(\frac{1}{\rho} - \frac{1}{\rho_0}\right) = 0, \quad U^2 = c^2, \tag{3.1a-d}$$

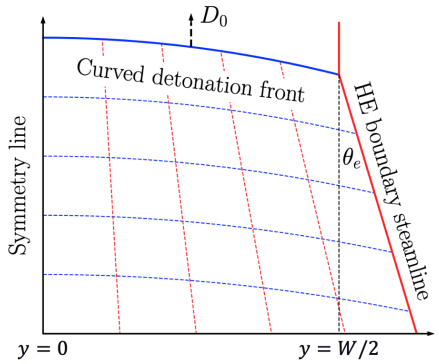


Figure 1: Shock-fitted, shock-attached frame of reference used for simulations of detonation propagation in 2-D, planar (slab) geometry. Boundary conditions are labeled, with outflow (extrapolation) condition on the south boundary.

where $U = u - D_0$ is the flow velocity in the wave-attached frame. Two additional constraints are derived from the 1-D steady traveling wave forms of equations (2.1). The first, called the "Master Equation", illustrates how reaction and compaction processes interact,

$$(c^2 - U^2)\frac{dU}{dx} = c^2\dot{\sigma}, \quad \dot{\sigma} = \sum_i \Lambda_i \sigma_i, \quad \sigma_i = -\left(\frac{1}{\rho c^2}\right)\frac{\partial e/\partial \lambda_i}{\partial e/\partial p}, \tag{3.2a-c}$$

where $x$ is the transformed, wave-attached coordinate, $c$ is the frozen sound speed, $\dot{\sigma}$ is the total thermicity, and $\sigma_i$ is the thermicity coefficient of $\lambda_i$, for $\lambda_i \in \{\lambda_s, \alpha_s\}$ and $\Lambda_i \in \{\Lambda, \mathcal{F}\}$ [4, 12]. In smooth regions of the flow, i.e. $dU/dx$ is finite, equation (3.2a) indicates that the CJ condition (3.1d) is satisfied only if the total thermicity vanishes simultaneously. Accordingly, we require $\dot{\sigma} = 0$ at the CJ state. A locus of steady flow $(\lambda_s, \alpha_s)$-states provides the final constraint for the porous HE CJ solution. The steady traveling wave forms of the reaction progress and volume fraction evolution equations (2.1d,e), i.e. $d\lambda_s/dx = \Lambda/U$ and $d\alpha_s/dx = \mathcal{F}/U$, respectively, may be combined, eliminating $dx/U$,

$$\frac{d\alpha_s}{d\lambda_s} = \frac{\mathcal{F}}{\Lambda} \quad \Longrightarrow \quad (k\mu)\frac{d\alpha_s}{\alpha_s(1-\alpha_s)} = (1-\lambda_s)^{-1/2}d\lambda_s, \tag{3.3a,b}$$

and integrated to obtain

$$\ln\left(\frac{\alpha_s}{1-\alpha_s}\right) = \ln\left(\frac{\alpha_{s0}}{1-\alpha_{s0}}\right) + \left(\frac{2}{k\mu}\right)\left(1-(1-\lambda_s)^{1/2}\right), \tag{3.4a}$$

$$\text{or} \quad \alpha_s = \frac{\omega}{1+\omega}, \quad \omega = \left(\frac{\alpha_{s0}}{1-\alpha_{s0}}\right)\exp\left[\frac{2}{k\mu}\left(1-(1-\lambda_s)^{1/2}\right)\right], \tag{3.4b}$$

which describes locus of $(\lambda_s, \phi_s)$ states in a steady flow for given $k\mu$. A shooting method is used to solve the non-linear system of equations.

The variation of $D_{CJ}$ with $k\mu$ is plotted in Fig. 2a for HE with 10% or 20% initial porosity, with corresponding $\lambda_{s,CJ}$ and $\alpha_{s,CJ}$ values shown in Fig. 2b. For $k\mu \leq 0.2$, both compaction and reaction processes reach equilibrium at the CJ state, i.e. $\alpha_{s,CJ} = 1$ and $\lambda_{s,CJ} = 1$, called the equilibrium CJ state. Since the pressures of detonation far exceed those required to fully compact granular HE, the equilibrium CJ response may be the most physically reasonable one [9]. As $k\mu$ is increased, $D_{CJ}$ increases monotonically before asymptotically approaching $D_{CJ}$ for non-porous HE. Note that in the limit of no compaction on the reaction zone scale, the wave speed does not depend on porosity. The value

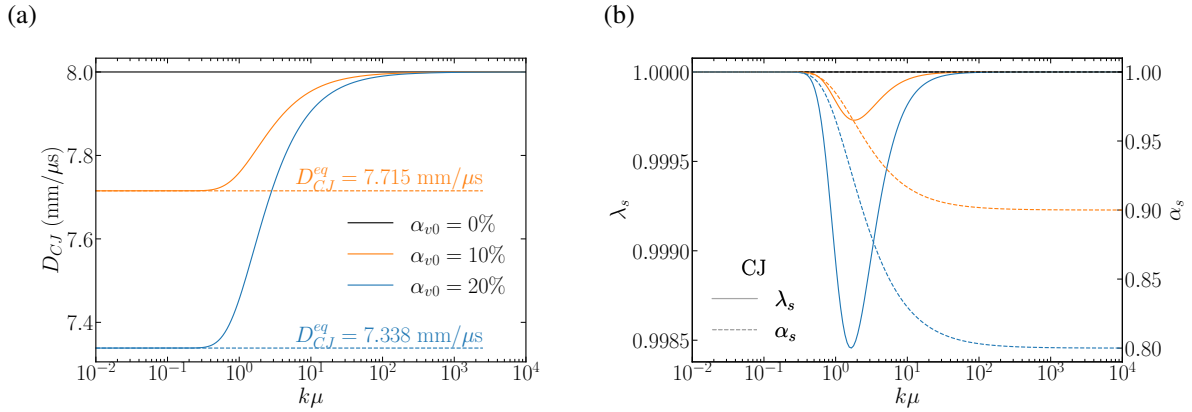


Figure 2: Chapman-Jouguet detonation properties for porous HE are shown as a functions of $k\mu$ for HE with 0%, 10% and 20% initial porosity. Shown in (a) is the variation of $D_{CJ}$, and in (b) the values of $\lambda_s$ and $\alpha_s$ at the CJ state.

of reaction progress at the CJ state varies non-monotonically with increasing $k\mu$, exhibiting minima near $k\mu \approx 2$ for the initial porosities shown.

One-dimensional CJ ZND detonation wave structures are shown in Fig. 3 for HE with different initial porosities and $k\mu$. For equilibrium CJ detonations, the length of the reaction zone increases with increasing initial porosity for fixed $k\mu$ (Fig. 3a). Lower CJ wave speeds result in reduced pressures and pressure-dependent reaction rates, leading to longer DDZ structures. For given initial porosity, the length of the reaction zone is nearly constant for equilibrium CJ detonations. Figure 3b compares the CJ ZND wave structures for two different initially porous HEs which share the same $D_{CJ} = 7.715$ mm/$\mu$s. Though the HE with 20% initial porosity with $k\mu = 2.837$ is not completely compacted or reacted at the CJ state (see Fig. 2b), the solid pressure $p_{s,CJ}$ is the same for the 10% and 20% initial porosities for their respective values of $k\mu$.

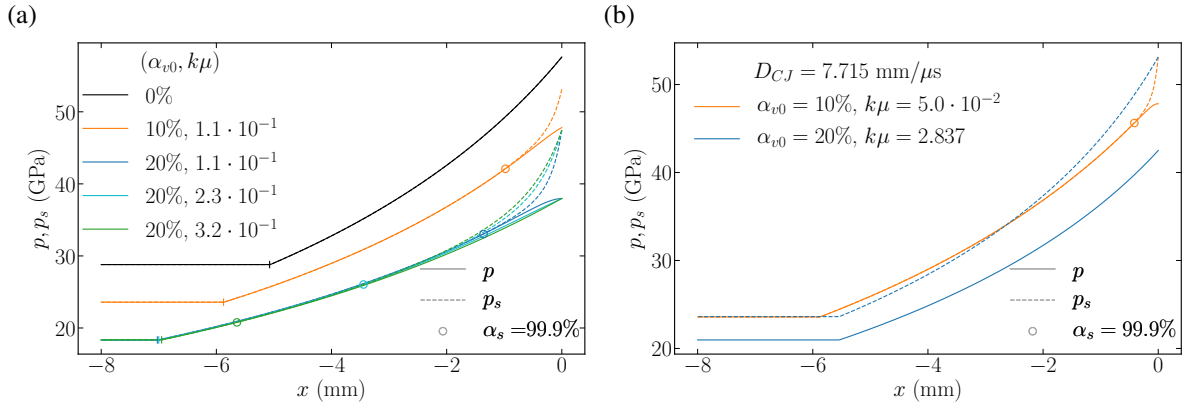


Figure 3: Spatial variations of pressure through 1-D, CJ, ZND waves in porous HE. The spatial variations of $p$ and $p_s$ are shown in (a) for equilibrium CJ detonation in initially porous and nonporous HE, and in (b) for HEs with different initial porosities but the same $D_{CJ}$.

Lateral yield of HE confinement in multi-dimensional detonation results in streamline divergence and detonation shock curvature (Fig. 4) [6]. For sufficiently weak HE confinement, the sonic locus intersects the detonation shock at the HE-confiner interface. The movement of the sonic locus into the reaction zone reduces the chemical energy available to support the detonation propagation, leading to reduced wave speeds. In general, the wave speed decreases as the charge size is reduced, known as the size

effect. A critical charge size exists below which detonation is quenched, known as the failure size. Size effect curves for unconfined, porous HE with different initial porosity and $k\mu$ are shown in figure 5. The size effect curves become increasingly sensitive to both initial porosity and compaction viscosity as the slab width is decreased (Fig. 5a). For given initial porosity, the solid pressure $p_s$ is sustained along a particle path for a longer period as $\mu$ is increased. Higher pressures drive increased reaction rates and energy release in the DDZ, leading to steady detonation propagation in smaller charges. For given $k\mu$, the detonation failure size increases with initial porosity. Detonation shocks and sonic loci are plotted in Fig. 6 for charges with $T/2 = 14.5$ mm, 19.0 mm and 27.5 mm. As the initial porosity increases, the shock curvature increases and the sonic locus moves further away from the shock.

In summary, we find the effects of porosity on steady detonation propagation to be significant and non-trivial. Using relatively simple models for the HE, we have explored how initial porosity and granular material compaction processes affect the physics of one- and multi-dimensional detonation propagation in porous HE.

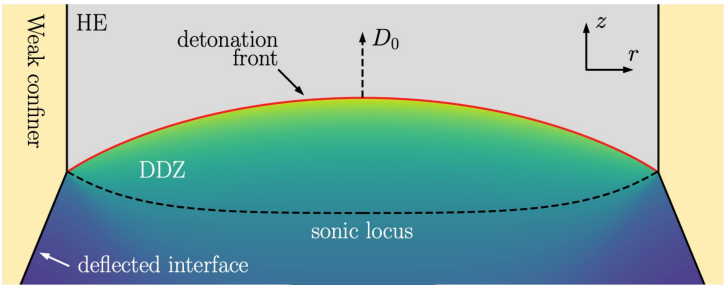


Figure 4: Flow field near the shock for two-dimensional, steady detonation propagation in HE with weak confinement.

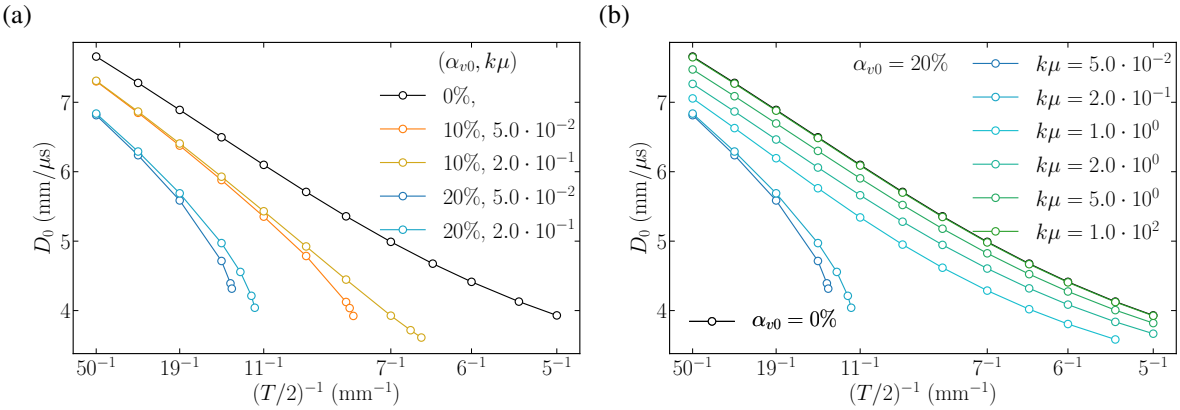


Figure 5: Size effect curves for HEs with different initial porosities and $k\mu$.

## References

[1] S.I. Jackson and M. Short. Scaling of detonation velocity in cylinder and slab geometries for ideal, insensitive and non-ideal explosives. *J. Fluid Mech.*, 773:224–266, 2015.

[2] E.K. Anderson, M. Short, S.J. Voelkel, G.A. Montoya, R.I. Chicas, and C. Chiquete. Influence of initial density on detonation propagation in a TATB-based high explosive. *Combust. Flame*, 273:113920, 2025.

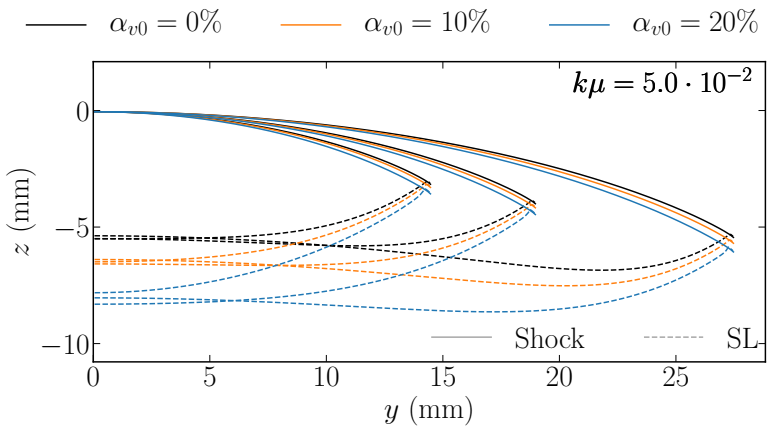


Figure 6: Detonation shock and sonic loci (SL) for HE with 0, 10% or 20% initial porosity and $k\mu = 0.05$. Slab widths shown include T/2 = 14.5, 19.0, and 27.5 mm.

[3] W. Fickett and W. C. Davis. *Detonation*. University of California Press, California, 1979.

[4] J.B. Bdzil and D.S. Stewart. The dynamics of detonation in explosive systems. *Annu. Rev. Fluid Mech.*, 39:263–292, 2007.

[5] M. Short, C. Chiquete, J.B. Bdzil, and J.J. Quirk. Detonation diffraction in a circular arc geometry of the insensitive high explosive PBX 9502. *Combust. Flame*, 196:129–143, 2018.

[6] M. Short and J.J. Quirk. High explosive detonation–confiner interactions. *Annu. Rev. Fluid Mech.*, 50:215–242, 2018.

[7] B.L. Wescott, D.S. Stewart, and W.C. Davis. Equation of state and reaction rate for condensed-phase explosives. *J. Appl. Phys.*, 98, 2005.

[8] A.K. Kapila, R. Menikoff, J.B. Bdzil, S.F. Son, and D.S. Stewart. Two-phase modeling of deflagration-to-detonation transition in granular materials: Reduced equations. *Phys. Fluids*, 13:3002–3024, 2001.

[9] J.B. Bdzil, R. Menikoff, S.F. Son, A.K. Kapila, and D.S. Stewart. Two-phase modeling of deflagration-to-detonation transition in granular materials: A critical examination of modeling issues. *Phys. Fluids*, 11:378–402, 1999.

[10] M. Short and J.J. Quirk. The effect of compaction of a porous material confiner on detonation propagation. *J. Fluid Mech.*, 834:434–463, 2018.

[11] J.A. Sáenz and D.S. Stewart. Modeling deflagration-to-detonation transition in granular explosive pentaerythritol tetranitrate. *J. Appl. Phys.*, 104, 2008.

[12] C.A. Eckett, J.J. Quirk, and J.E. Shepherd. The role of unsteadiness in direct initiation of gaseous detonations. *J. Fluid Mech.*, 421:147–183, 2000.